J. Appl. Comput. Mech., 6(1) (2020) 90-104
DOI: 10.22055/JACM.2019.28245.1468

ISSN: 2383-4536
jacm.scu.ac.ir

M&MoCS

Shahid Chamran
University of Ahvaz

Journal of
Applied and Computational Mechanics

Research Paper

Stress Redistribution Analysis of Piezomagnetic Rotating Thick-Walled Cylinder with Temperature-and Moisture-Dependent Material Properties

Mahdi Saadatfar

Department of Mechanical Engineering, University of Qom
Qom, P.O. Box 3716146611, Iran, Email: m.saadatfar@qom.ac.ir

Received January 15 2019; Revised April 09 2019; Accepted for publication April 09 2019.
Corresponding author: Mahdi Saadatfar (m.saadatfar@qom.ac.ir)

Abstract. In this article, the problem of time-dependent stress redistribution of a piezomagnetic rotating thick-walled cylinder under an axisymmetric hygro-thermo-magneto-electro-mechanical loading is analyzed analytically for the condition of plane strain. Using the constitutive equations, a differential equation is found in which there are creep strains. Primarily, eliminating creep strains, an analytical solution for the primitive electric and magnetic potential in addition to stresses is obtained. Then, creep strains are kept and creep stress rates are found by utilizing Norton's law and Prandtl-Reuss equations for steady-state hygrothermal boundary condition. Lastly, the history of stresses and radial displacement as well as magnetic and potential fields during the time is obtained using an iterative method. In the numerical examples, the effect of angular velocity, hygrothermal loading and thermal and moisture concentration dependency of elastic constants is investigated comprehensively.

Keywords: Hollow cylinder, Piezomagnetic, Hygrothermal condition, Time-dependent analysis.

1. Introduction

Todays, intelligent materials have ever increasing usages in new engineering areas. Piezomagnetics are two-phase composites which are made of piezoelectrics and magneto-elastic materials. In these materials, there is an extensive coupling effect between electrical and magnetic fields that there is not in a single-phase material. Besides, applying an electric field or magnetic field as well as mechanical load may results in an elastic deformation in these materials. Owing to the usage of intelligent structures in various working conditions, interactions of humidity, thermal field, electric field, magnetic field and elastic field on the response of these materials must be analyzed. Due to inherent viscoelastic properties of smart materials, to have the best design, time-dependent creep analysis should be done for actuators employed for high-precision positioning and load-bearing usages.

In the area of hygrothermal analysis, several analyses are carried out in the literature to discover the multiphysical behavior of smart materials. The hygrothermal analysis of laminated piezoelectric plates was presented by Smittakorn and Heyliger [1]. The hygrothermal behavior of laminated piezoelectric plates in addition to shells was considered by Raja et al. [2]. Allam et al. [3] presented analyzed the interaction of electric field, elastic deformation, and hygrothermal condition in hollow and solid piezoelectric cylinders. Saadatfar and Aghaie-Khafri [4] analyzed hygrothermal stresses in a functionally graded magneto-electro-elastic (FGMEE) thick-walled sphere using an analytical method. The hygrothermal problem of a long functionally graded material (FGM) cylindrical shell bonded to functionally graded piezoelectric material (FGPM) sensor and actuators is solved analytically by Saadatfar and Aghaie-Khafri [5]. Then, Saadatfar and Aghaie-Khafri [6] and Saadatfar [7] presented hygro-thermal and magneto-hygrothermal analysis of a

Published online: July 10 2019

short length cylindrical shell made of FGM integrated with FGPM layers. Zenkour [8] presented a solution for a piezoelectric functionally graded fiber-reinforced thick-walled cylinder in hygrothermal environmental condition. Vinyas and Kattimani [9] investigated the stress problem of MEE plate in hygrothermal environment using the finite element method.

In the area of analysis of piezomagnetic cylinders, Hou and Leung [10] analyzed the transient responses of piezomagnetic thick-walled cylinder in plane strain condition. Wang and Ding [11] investigated the transient behavior of a non-homogeneous piezomagnetic thick-walled cylinder in axisymmetric plane strain condition. Babaei and Chen [12] presented an analytical solution for static problem of a long piezomagnetic hollow and solid rotating cylinder. Ootao and Ishihara [13] derived an exact solution for the problem of transient thermal stress in a multilayered piezomagnetic thick-walled cylinder. Akbarzadeh and Chen [14] investigated the responses of hollow and solid piezomagnetic cylinders in hygrothermal loading condition using an analytical method.

Some authors have considered the creep analysis in cylinders. The time-dependent stress redistribution of a FGM hollow cylinder subjected thermo-magneto-mechanical loads was studied by Loghman et al. [15]. Singh and Gupta [16] studied the steady-state creep behavior of an anisotropic FGM cylinder. Using transition theory, the creep stresses redistribution in a hollow cylinder under mechanical pressure was investigated by Sharma et al. [17]. Utilizing Bailey-Norton creep model, the time-dependent creep behavior of an exponentially FGM rotating hollow cylinder is analyzed by Loghman and Atabakhshian [18]. Jamian et al. [19] carried out the creep analysis for a FGM hollow cylinder under thermo-mechanical loads. Nejad and Kashkoli [20] studied the time-dependent thermo-elastic creep response for isotropic rotating FGM cylindrical shell. Considering residual stresses, Singh and Gupta [21] presented the steady-state creep analysis in a FGM composite hollow cylinder under mechanical load. The steady-state creep behavior of a rotating FGM thick-walled cylindrical shell in plane strain condition was investigated by Nejad et al. [22]. Kashkoli et al. [23, 24] analyzed the time-dependent thermo-elastic creep response of functionally graded and homogeneous thick-walled cylinder. Sharma el al. [25] considered the creep response problem of a FGM cylinder in torsion and thermo-mechanical loading. Bakhshizadeh et al. [26] carried out time-dependent hygrothermal creep investigation of pressurized rotating FGM cylindrical shells subjected to uniform magnetic field. For piezoelectric cylinders: A semi-analytical solution to achieve the stresses redistribution of a rotating FGPM hollow cylinder during creep evolution was presented by Ghorbanpour Arani et al. [27]. Ghorbanpour Arani et al. [28] analyzed the time-dependent thermo-elastic creep progress in a piezoelectric hollow cylinder using a semi-analytical method.

Literature review in the area of creep analysis of intelligent materials implies that there is no published research about time-dependent creep evolution of a piezomagnetic hollow cylinder in hygrothermal condition. So, this article makes the first try to derive an analytical solution for the problem of creep response of piezomagnetic thick-walled cylinder employing the Prandtl-Reuss equations as well as Norton's law. The main aim of this research is to reveal the influences of conceivable interactions of various physical area on the creep response of piezomagnetic structure.

2. Basic Formulation of the Problem

A rotating piezomagnetic hollow cylinder polarized and magnetized through the radial direction and a cylindrical coordinate system (r, θ , z) are considered as shown in Fig. 1. Due to symmetry and plane strain condition, nonzero components of electromagnetic fields, deformation and hygrothermal fields are function of radius.

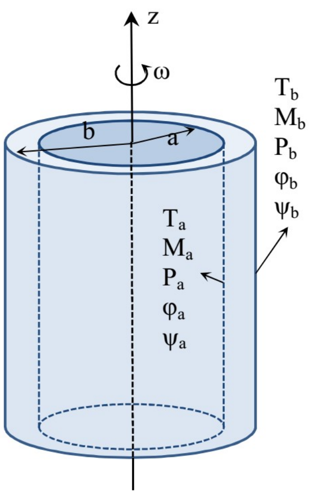

Fig. 1. Piezomagnetic hollow cylinder

2.1 Basic equations of the piezomagnetic cylinder

It is supposed that total strains are sum of magnetic, electric, hygrothermal, elastic and creep strains. Thus, the stress-strain relations can be presented in the following form [14, 27]:

$$\sigma_r = c_{11}\frac{\partial u}{\partial r} + c_{12}\frac{u}{r} + e_{11}\frac{\partial \phi}{\partial r} + q_{11}\frac{\partial \psi}{\partial r} - \lambda_1 T - \zeta_1 M - c_{11}\varepsilon_{rr}^c - c_{12}\varepsilon_{\theta\theta}^c \tag{1.a}$$

$$\sigma_\theta = c_{12}\frac{\partial u}{\partial r} + c_{22}\frac{u}{r} + e_{12}\frac{\partial \phi}{\partial r} + q_{12}\frac{\partial \psi}{\partial r} - \lambda_2 T - \zeta_2 M - c_{12}\varepsilon_{rr}^c - c_{22}\varepsilon_{\theta\theta}^c \tag{1.b}$$

$$D_r = e_{11}\frac{\partial u}{\partial r} + e_{12}\frac{u}{r} - \beta_{11}\frac{\partial \phi}{\partial r} - \varepsilon_{11}\frac{\partial \psi}{\partial r} + p_1 T + \chi_1 M - e_{11}\varepsilon_{rr}^c - e_{12}\varepsilon_{\theta\theta}^c, \tag{1.c}$$

$$B_r = q_{11}\frac{\partial u}{\partial r} + q_{12}\frac{u}{r} - \varepsilon_{11}\frac{\partial \phi}{\partial r} - d_{11}\frac{\partial \psi}{\partial r} + m_1 T + \gamma_1 M - q_{11}\varepsilon_{rr}^c - q_{12}\varepsilon_{\theta\theta}^c \tag{1.d}$$

where:

$$\lambda_1 = c_{11}\alpha_r + c_{12}\alpha_\theta, \qquad \lambda_2 = c_{12}\alpha_r + c_{22}\alpha_\theta \tag{2.a}$$

$$\zeta_1 = c_{11}\beta_r + c_{12}\beta_\theta, \qquad \zeta_2 = c_{12}\beta_r + c_{22}\beta_\theta \tag{2.b}$$

without body forces, electric charge and electric current densities, the equations of equilibrium, electrostatic and magnetostatic for a rotating piezomagnetic hollow cylinder are as [14, 29, 30]:

$$\frac{\partial \sigma_r}{\partial r} + \frac{(\sigma_r - \sigma_\theta)}{r} + \rho r \omega^2 = 0. \tag{3.a}$$

$$\frac{\partial D_r}{\partial r} + \frac{D_r}{r} = 0, \tag{3.b}$$

$$\frac{\partial B_r}{\partial r} + \frac{B_r}{r} = 0. \tag{3.c}$$

2.2 Basic differential equation of the problem

Solving Eqs. (3.b) and (3.c), gives:

$$D_r = \frac{A_1}{r}, \tag{4.a}$$

$$B_r = \frac{A_2}{r}. \tag{4.b}$$

where A_1 and A_2 are unknown constants. Using Eq. (4) into Eqs. (1.c) and (1.d), after rearranging, gives:

$$\frac{\partial \phi(r)}{\partial r} = \left(L_1\frac{\partial u}{\partial r} + L_2\frac{u}{r} + L_3\frac{A_2}{r} + L_4 T + L_6 M - L_5\frac{A_1}{r} - L_1\varepsilon_{rr}^c - L_2\varepsilon_{\theta\theta}^c \right) \tag{5.a}$$

$$\frac{\partial \psi(r)}{\partial r} = \left(P_1\frac{\partial u}{\partial r} + P_2\frac{u}{r} + P_3\frac{A_1}{r} + P_4 T + P_6 M - P_5\frac{A_2}{r} - P_1\varepsilon_{rr}^c - P_2\varepsilon_{\theta\theta}^c \right) \tag{5.b}$$

where:

$$\begin{aligned} &L_1 = \frac{e_{11}d_{11} - \varepsilon_{11}q_{11}}{\beta_{11}d_{11} - \varepsilon^2{}_{11}}, \quad L_2 = \frac{e_{12}d_{11} - \varepsilon_{11}q_{12}}{\beta_{11}d_{11} - \varepsilon^2{}_{11}}, \quad L_3 = \frac{\varepsilon_{11}}{\beta_{11}d_{11} - \varepsilon^2{}_{11}}, \quad L_4 = \frac{d_{11}p_1 - \varepsilon_{11}m_1}{\beta_{11}d_{11} - \varepsilon^2{}_{11}}, \\ &L_5 = \frac{d_{11}}{\beta_{11}d_{11} - \varepsilon^2{}_{11}}, \quad L_6 = \frac{d_{11}\chi_1 - \varepsilon_{11}\gamma_1}{\beta_{11}d_{11} - \varepsilon^2{}_{11}}, \quad P_1 = \frac{q_{11}\beta_{11} - \varepsilon_{11}e_{11}}{\beta_{11}d_{11} - \varepsilon^2{}_{11}}, \quad P_2 = \frac{q_{12}\beta_{11} - e_{12}\varepsilon_{11}}{\beta_{11}d_{11} - \varepsilon^2{}_{11}}, \\ &P_3 = \frac{\varepsilon_{11}}{\beta_{11}d_{11} - \varepsilon^2{}_{11}}, \quad P_4 = \frac{\beta_{11}m_1 - \varepsilon_{11}p_1}{\beta_{11}d_{11} - \varepsilon^2{}_{11}}, \quad P_5 = \frac{\beta_{11}}{\beta_{11}d_{11} - \varepsilon^2{}_{11}}, \quad P_6 = \frac{\beta_{11}\gamma_1 - \varepsilon_{11}\chi_1}{\beta_{11}d_{11} - \varepsilon^2{}_{11}}, \end{aligned} \tag{6}$$

Using Eq. (5) into Eqs. (1.a) and (1.b), gives:

$$\sigma_r = C_1\frac{\partial u}{\partial r} + C_2\frac{u}{r} + C_3\frac{A_2}{r} + C_4\frac{A_1}{r} + C_5 T + C_6 M - \lambda_1 T - \zeta_1 M - C_1\varepsilon_{rr}^c - C_2\varepsilon_{\theta\theta}^c, \tag{7.a}$$

$$\sigma_\theta = E_1\frac{\partial u}{\partial r} + E_2\frac{u}{r} + E_3\frac{A_2}{r} + E_4\frac{A_1}{r} + E_5 T + E_6 M - \lambda_2 T - \zeta_2 M - E_1\varepsilon_{rr}^c - E_1\varepsilon_{\theta\theta}^c \tag{7.b}$$

where:

$$\begin{aligned}
&C_1 = c_{11} + e_{11}L_1 + q_{11}P_1, && C_2 = c_{12} + e_{11}L_2 + q_{11}P_2, && C_3 = e_{11}L_3 - q_{11}P_5,\\
&C_4 = -e_{11}L_5 + q_{11}P_3, && C_5 = e_{11}L_4 + q_{11}P_4, && C_6 = e_{11}L_6 + q_{11}P_6,\\
&E_1 = c_{12} + e_{12}L_1 + q_{12}P_1, && E_2 = c_{22} + e_{12}L_2 + q_{12}P_2, && E_3 = e_{12}L_3 - q_{12}P_5,\\
&E_4 = -e_{12}L_5 + q_{12}P_3, && E_5 = e_{12}L_4 + q_{12}P_4, && E_6 = e_{12}L_6 + q_{12}P_6
\end{aligned} \tag{8}$$

Using Eqs. (7) into Eq. (3.a), the equilibrium equation is now can be rewritten as:

$$\begin{aligned}
&\frac{\partial^2 u}{\partial r^2} + \frac{1}{r}M_1\frac{\partial u}{\partial r} + \frac{1}{r^2}M_2 u = (M_3 + M_4)\frac{T}{r} + (-M_5 + M_6)\frac{\partial T}{\partial r} + M_7\frac{A_2}{r^2} + M_8\frac{A_1}{r^2}\\
&+(M_9 + M_{10})\frac{M}{r} + (-M_{11} + M_{12})\frac{\partial M}{\partial r} - M_{13}r + M_{14}r^{-1}\varepsilon_{rr}^c + \frac{\partial \varepsilon_{rr}^c}{\partial r} + M_{15}r^{-1}\varepsilon_{\theta\theta}^c + M_{16}\frac{\partial \varepsilon_{\theta\theta}^c}{\partial r}
\end{aligned} \tag{9}$$

where:

$$\begin{aligned}
&M_1 = \frac{C_1 + C_2 - E_1}{C_1}, \quad M_2 = \frac{-E_2}{C_1}, \quad M_3 = \frac{(\lambda_1 - \lambda_2)}{C_1}, \quad M_4 = \frac{E_5 - C_5}{C_1},\\
&M_5 = \frac{C_5}{C_1}, \quad M_6 = \frac{\lambda_1}{C_1}, \quad M_7 = \frac{E_3}{C_1}, \quad M_8 = \frac{E_4}{C_1}, \quad M_9 = \frac{(\zeta_1 - \zeta_2)}{C_1}, \quad M_{10} = \frac{E_6 - C_6}{C_1},\\
&M_{11} = \frac{C_6}{C_1}, \quad M_{12} = \frac{\zeta_1}{C_1}, \quad M_{13} = \frac{\rho\omega^2}{C_1}, \quad M_{14} = \frac{2C_1 - 2E_1}{C_1}, \quad M_{15} = \frac{2C_2 - 2E_2}{C_1}, \quad M_{16} = \frac{C_2}{C_1}
\end{aligned} \tag{10}$$

The cylinder is assumed under mechanical pressure, temperature change, moisture concentration change, electric potential and magnetic potential at the inside and outside surface. These boundary conditions can be expressed as:

$$\begin{aligned}
&\sigma_r\big|_{r=a} = -p_a, && \sigma_r\big|_{r=b} = -p_b,\\
&\phi\big|_{r=a} = \phi_a, && \phi\big|_{r=b} = \phi_b,\\
&\psi\big|_{r=a} = \psi_a, && \psi\big|_{r=b} = \psi_b.\\
&T\big|_{r=a} = T_a, && T\big|_{r=b} = T_b,\\
&M\big|_{r=a} = M_a, && M\big|_{r=b} = M_b,
\end{aligned} \tag{11}$$

3. Solution of the Equations

3.1 Temperature and moisture concentration problem

In an uncoupled hygrothermal analysis, the distributions of temperature and moisture concentration are determined independently [31]. The Fourier heat conduction equation as well as Fickian moisture diffusion equation without source of heat and moisture for a cylinder in axisymmetric steady-state condition is as [14, 32, 33]:

$$\frac{1}{r}\frac{\partial}{\partial r}\left(rk^T\frac{\partial T}{\partial r}\right) = 0, \tag{12.a}$$

$$\frac{1}{r}\frac{\partial}{\partial r}\left(rk^C\frac{\partial M}{\partial r}\right) = 0, \tag{12.b}$$

Integrating Eq. (12) twice gives:

$$\begin{aligned}
&T(r) = W_1\ln(r) - W_2,\\
&M(r) = S_1\ln(r) - S_2.
\end{aligned} \tag{13}$$

The unknown constants can be determined using hygrothermal boundary conditions as:

$$W_1 = \frac{T_b - T_a}{\ln(b) - \ln(a)}, \qquad W_2 = \frac{T_b - T_a}{\ln(b) - \ln(a)}\ln(b) - T_b \tag{14.a}$$

$$S_1 = \frac{M_b - M_a}{\ln(b) - \ln(a)}, \qquad S_2 = \frac{M_b - M_a}{\ln(b) - \ln(a)}\ln(b) - M_b. \tag{14.b}$$

3.2 Primitive hygrothermal analysis of the piezomagnetic cylinder

To find initial stresses, discounting creep strains in Eq. (9), one has:

$$\begin{aligned}&\frac{\partial^2 u}{\partial r^2}+\frac{M_1}{r}\frac{\partial u}{\partial r}+\frac{M_2}{r^2}u=\left(-M_3W_2-M_9S_2-M_4W_2-M_{10}S_2-M_5W_1+M_6W_1-M_{11}S_1+M_{12}S_2\right)r^{-1}\\&+\left(W_1M_3+S_1M_9+W_1M_4+S_1M_{10}\right)\ln(r)r^{-1}+M_7A_2r^{-2}+M_8A_1r^{-2}-M_{13}r\end{aligned} \tag{15}$$

The complete solution of Eq. (15) can be written as:

$$\begin{aligned}&u=B_1r^{m_1}+B_2r^{m_2}+\left(B_3\right)r+B_6r^3+B_7A_2+B_8A_1-\frac{B_5r}{(1-m_1)(m_2-m_1)}\left(\ln(r)-\frac{1}{1-m_1}\right)\\&+\frac{B_5r}{(1-m_2)(m_2-m_1)}\left(\ln(r)-\frac{1}{1-m_2}\right)\end{aligned} \tag{16}$$

where B_1 and B_2 are unknown constants and:

$$\begin{aligned}&m_{1,2}=\frac{1}{2}\left(-(M_1-1)\pm\sqrt{(M_1-1)^2-4M_2}\right),\quad B_8=\frac{M_8}{M_2},\quad B_7=\frac{M_7}{M_2},\\&B_3=\frac{-M_4W_2-M_{10}S_2-M_3W_2-M_9S_2-M_{11}S_1+M_{12}S_2-M_5W_1+M_6W}{M_1+M_2},\\&B_5=\frac{W_1\left(M_4\right)+S_1\left(M_{10}\right)+W_1\left(M_3\right)+S_1\left(M_9\right)}{+M_1+M_2},\quad B_6=\frac{-M_{13}}{6+3M_1+M_2},\end{aligned} \tag{17}$$

Using Eq. (16) and integrating Eq. (5), one has:

$$\begin{aligned}&\phi(r)=L_1\left(B_1r^{m_1}+B_2r^{m_2}+B_3r+B_5+B_6r^3-\frac{B_5}{(1-m_1)(m_2-m_1)}\left(r\ln(r)-2r-\frac{r}{1-m_1}\right)\right.\\&\left.-\frac{B_5}{(1-m_2)(m_2-m_1)}\left(r\ln(r)-2r-\frac{r}{1-m_2}\right)\right)+L_2\left(\frac{B_1}{m_1}r^{m_1}+\frac{B_2}{m_2}r^{m_2}+B_3r+\frac{B_6}{3}r^3+\left(B_7A_2+B_8A_1\right)\ln(r)\right.\\&\left.-\frac{B_5r}{(1-m_1)(m_2-m_1)}\left(\ln(r)-1-\frac{1}{1-m_1}\right)+\frac{B_5r}{(1-m_2)(m_2-m_1)}\left(\ln(r)-1-\frac{1}{1-m_2}\right)\right)\\&+L_4\left(W_1r\ln(r)-W_1r+W_2r\right)+L_6\left(S_1r\ln(r)-S_1\,\mathrm{r}+S_2r\right)+\left(-L_5A_1+L_3A_2\right)\ln(r)+Z_1\end{aligned} \tag{18}$$

where Z_1 is an unknown constant. With the similar method, ψ is achieved as:

$$\begin{aligned}&\psi(r)=P_1\left(B_1r^{m_1}+B_2r^{m_2}+B_3r+B_5+B_6r^3-B_5\frac{1}{(1-m_1)(m_2-m_1)}\left(r\ln(r)-2\,\mathrm{r}-\frac{r}{1-m_1}\right)\right.\\&\left.-B_5\frac{1}{(1-m_2)(m_2-m_1)}\left(r\ln(r)-2\,\mathrm{r}-\frac{r}{1-m_2}\right)\right)+P_2\left(\frac{B_1}{m_1}r^{m_1}+\frac{B_2}{m_2}r^{m_2}+B_3r+\frac{B_6}{3}r^3+\left(B_7A_2+B_8A_1\right)\ln(r)\right.\\&\left.-\frac{B_5r}{(1-m_1)(m_2-m_1)}\left(\ln(r)-1-\frac{1}{1-m_1}\right)+\frac{B_5r}{(1-m_2)(m_2-m_1)}\left(\ln(r)-1-\frac{1}{1-m_2}\right)\right)+P_4\left(W_1r\ln(r)-W_1r+W_2r\right)\\&+P_6\left(S_1r\ln(r)-S_1\,\mathrm{r}+S_2r\right)+\left(-P_5A_1+P_3A_2\right)\ln(r)+Z_2\end{aligned} \tag{19}$$

where Z_2 is an unknown constant. Using Eqs. (16) and (13) into Eq. (7), the radial and hoop stresses are obtained as:

$$\begin{aligned}&\sigma_r=C_1\left(B_1m_1r^{m_1-1}+B_2m_2r^{m_2-1}+B_3+3B_6r^2-\frac{B_5}{(1-m_1)(m_2-m_1)}\left(\ln(r)-\frac{1}{1-m_1}+1\right)\right.\\&\left.+\frac{B_5}{(1-m_2)(m_2-m_1)}\left(\ln(r)-\frac{1}{1-m_2}+1\right)\right)+C_2\left(B_1r^{m_1}+B_2r^{m_2}+B_3r+B_6r^3+B_7A_2+B_8A_1\right.\\&\left.-\frac{B_5r}{(1-m_1)(m_2-m_1)}\left(\ln(r)-\frac{1}{1-m_1}\right)+\frac{B_5r}{(1-m_2)(m_2-m_1)}\left(\ln(r)-\frac{1}{1-m_2}\right)\right)\\&+C_3\frac{A_2}{r}+C_4\frac{A_1}{r}+\left(C_5-\lambda_1\right)\left(W_1\ln(r)+W_2\right)+\left(C_6-\zeta_1\right)\left(S_1\ln(r)+S_2\right)\end{aligned} \tag{20}$$

$$\begin{aligned}\sigma_\theta = E_1\Bigg(& B_1 m_1 r^{m_1-1} + B_2 m_2 r^{m_2-1} + B_3 + 3B_6 r^2 - \frac{B_5}{(1-m_1)(m_2-m_1)}\left(\ln(r) - \frac{1}{1-m_1} + 1\right)\\ &+ \frac{B_5}{(1-m_2)(m_2-m_1)}\left(\ln(r) - \frac{1}{1-m_2} + 1\right)\Bigg) + E_2\Big(B_1 r^{m_1} + B_2 r^{m_2} + B_3 r + B_6 r^3 + B_7 A_2 + B_8 A_1\\ &- \frac{B_5 r}{(1-m_1)(m_2-m_1)}\left(\ln(r) - \frac{1}{1-m_1}\right) + \frac{B_5 r}{(1-m_2)(m_2-m_1)}\left(\ln(r) - \frac{1}{1-m_2}\right)\Big)\\ &+ E_3\frac{A_2}{r} + E_4\frac{A_1}{r} + \left(E_5 - \lambda_1\right)\left(W_1\ln(r) + W_2\right) + \left(E_6 - \zeta_1\right)\left(S_1\ln(r) + S_2\right)\end{aligned} \tag{21}$$

Utilizing the mechanical and electromagnetic boundary conditions, the unknown constants A_1, A_2, B_1, B_2, Z_1 and Z_2 can be determined by solving a system of linear algebraic equations. The details of this system and components of matrixes are not present here for the sake of brevity. Solving this system results in obtaining the initial stresses, electric potential, magnetic potential and displacement analytically at zero time.

3.3 Time-dependent creep analysis of piezomagnetic cylinder

Assuming the steady-state hygrothermal condition, differentiation Eq. (9) with respect to time yields:

$$\frac{\partial^2 \dot{u}}{\partial r^2} + \frac{1}{r}M_1\frac{\partial \dot{u}}{\partial r} + \frac{1}{r^2}M_2\dot{u} = +M_7\frac{\dot{A}_2}{r^2} + M_8\frac{\dot{A}_1}{r^2} + M_{14}r^{-1}\dot{\varepsilon}^c_{rr} + \frac{\partial \dot{\varepsilon}^c_{rr}}{\partial r} + M_{15}r^{-1}\dot{\varepsilon}^c_{\theta\theta} + M_{16}\frac{\partial \dot{\varepsilon}^c_{\theta\theta}}{\partial r} \tag{22}$$

Well-known Prandtl-Reuss equations relate the creep rates to the stresses as follows [34]:

$$\begin{aligned}\dot{\varepsilon}^c_r &= \frac{\dot{\varepsilon}^c_e}{\sigma_e}(\sigma_r - 0.5(\sigma_\theta + \sigma_z))\\ \dot{\varepsilon}^c_\theta &= \frac{\dot{\varepsilon}^c_e}{\sigma_e}(\sigma_\theta - 0.5(\sigma_r + \sigma_z))\\ \dot{\varepsilon}^c_z &= \frac{\dot{\varepsilon}^c_e}{\sigma_e}(\sigma_z - 0.5(\sigma_\theta + \sigma_r))\end{aligned} \tag{23}$$

Norton's law is considered as the creep constitutive model as [34]:

$$\begin{aligned}&\dot{\varepsilon}^c_e = B(\mathrm{r})\sigma_e^{n(\mathrm{r})}\\ &B(\mathrm{r}) = b_0 r^{b_1},\ n(\mathrm{r}) = \mathrm{n}_0\end{aligned} \tag{24}$$

where b_0,b_1 and n_0 are constants. Regarding the plane strain condition and substituting Eq. (24) into Eq. (23) gives:

$$\begin{aligned}\dot{\varepsilon}^c_r &= -\frac{3B(\mathrm{r})}{4}\sigma_e^{n_0-1}\left(\sigma_\theta - \sigma_r\right)\\ \dot{\varepsilon}^c_\theta &= \frac{3B(\mathrm{r})}{4}\sigma_e^{n_0-1}\left(\sigma_\theta - \sigma_r\right)\\ \dot{\varepsilon}^c_z &= 0\end{aligned} \tag{25}$$

The Von Mises equivalent stress is presented as:

$$\sigma_e = \frac{1}{\sqrt{2}}\sqrt{(\sigma_\theta - \sigma_r)^2 + (\sigma_\theta - \sigma_\phi)^2 + (\sigma_\phi - \sigma_r)^2} = \frac{\sqrt{3}}{2}(\sigma_\theta - \sigma_r) \tag{26}$$

Now, Eqs. (25.a) and (25.b) are:

$$\begin{aligned}\dot{\varepsilon}^c_{rr} &= -\frac{\sqrt{3}}{2}b_0 r^{b_1}\sigma_e^{n_0}\\ \dot{\varepsilon}^c_{\theta\theta} &= \frac{\sqrt{3}}{2}b_0 r^{b_1}\sigma_e^{n_0}\end{aligned} \tag{27}$$

Using Eq. (27) into Eq. (22), one gets:

$$\frac{\partial^2 \dot{u}}{\partial r^2} + \frac{1}{r}M_1\frac{\partial \dot{u}}{\partial r} + \frac{1}{r^2}M_2\dot{u} = \frac{M_7\dot{A}_2}{r^2} + \frac{M_8\dot{A}_1}{r^2} + \frac{\sqrt{3}}{2}b_0 r^{b_1-1}\sigma_e^{n_0}\left(M_{15} + M_{16}b_1 - M_{14} - b_1\right) + \left(M_{16} - 1\right)\frac{\sqrt{3}}{2}b_0 r^{b_1}\frac{\partial \sigma_e^{n_0}}{\partial r} \tag{28}$$

By the same way as in previous section, the solution can be written as:

$$\dot{u} = D_1 r^{m_1} + D_2 r^{m_2} + G_{11} r^{m_1} + G_{21} r^{m_2} + B_7 \dot{A}_2 + B_8 \dot{A}_1 \tag{29}$$

where $G_{11}(r)$ and $G_{21}(r)$ can be achieved using the method of variation of parameters as [35]:

$$\begin{aligned} G_{11}(\mathrm{r}) &= \frac{\sqrt{3}}{2}\frac{b_0}{m_2 - m_1}\int\left\{ r^{b_1 - m_1}\sigma_e^{n_0}\left(M_{15} + M_{16}b_1 - M_{14} - b_1\right) + \left(M_{16} - 1\right) r^{b_1 - m_1 + 1}\frac{\partial \sigma_e^{n_0}}{\partial r}\right\} dr \\ G_{21}(\mathrm{r}) &= -\frac{\sqrt{3}}{2}\frac{b_0}{m_2 - m_1}\int\left\{ r^{b_1 - m_2}\sigma_e^{n_0}\left(M_{15} + M_{16}b_1 - M_{14} - b_1\right) + \left(M_{16} - 1\right) r^{b_1 - m_2 + 1}\frac{\partial \sigma_e^{n_0}}{\partial r}\right\} dr \end{aligned} \tag{30}$$

The details of the variation of parameters method are not explained here for briefness. Now, rates of stresses, electric potential and magnetic potential are obtained by differentiation Eqs. (7) and (5) with respect to time as:

$$\dot{\sigma}_r = C_1 \frac{\partial \dot{u}}{\partial r} + C_2 \frac{\dot{u}}{r} + C_3 \frac{\dot{A}_2}{r} + C_4 \frac{\dot{A}_1}{r} + (C_1 - C_2)\frac{\sqrt{3}}{2} b_0 r^{b_1} \sigma_e^{n_0}, \tag{31.a}$$

$$\dot{\sigma}_\theta = E_1 \frac{\partial \dot{u}}{\partial r} + E_2 \frac{\dot{u}}{r} + E_3 \frac{\dot{A}_2}{r} + E_4 \frac{\dot{A}_1}{r} + (E_1 - E_2)\frac{\sqrt{3}}{2} b_0 r^{b_1} \sigma_e^{n_0}, \tag{31.b}$$

$$\frac{\partial \dot{\phi}}{\partial r} = L_1 \frac{\partial \dot{u}}{\partial r} + L_2 \frac{\dot{u}}{r} - L_5 \frac{\dot{A}_1}{r} + L_3 \frac{\dot{A}_2}{r} - L_1 \dot{\varepsilon}_{rr}^c - L_2 \dot{\varepsilon}_{\theta\theta}^c \tag{31.c}$$

$$\frac{\partial \dot{\psi}}{\partial r} = P_1 \frac{\partial \dot{u}}{\partial r} + P_2 \frac{\dot{u}}{r} + P_3 \frac{\dot{A}_1}{r} - P_5 \frac{\dot{A}_2}{r} - P_1 \dot{\varepsilon}_{rr}^c - P_2 \dot{\varepsilon}_{\theta\theta}^c \tag{31.d}$$

Using Eq. (29) into Eq. (31) and integrating Eqs. (31.c) and (31.d), after rearranging, gives:

$$\begin{aligned} \dot{\sigma}_r =& D_1\left(m_1 C_1 + C_2\right) r^{m_1 - 1} + D_2\left(m_2 C_1 + C_2\right) r^{m_2 - 1} + \left(C_2 B_8 + C_4\right)\frac{\dot{A}_1}{r} \\ &+ \left(C_2 B_7 + C_3\right)\frac{\dot{A}_2}{r} + C_1\left(\frac{\partial G_{11}}{\partial r} r^{m_1} + G_{11} m_1 r^{m_1 - 1} + \frac{\partial G_{21}}{\partial r} r^{m_2} + G_{21} m_2 r^{m_2 - 1}\right) \\ &+ C_2\left(G_{11} r^{m_1 - 1} + G_{21} r^{m_2 - 1}\right) + \left(C_1 - C_2\right)\frac{\sqrt{3}}{2} b_0 r^{b_1} \sigma_e^{n_0} \end{aligned} \tag{32.a}$$

$$\begin{aligned} \dot{\sigma}_\theta =& D_1\left(m_1 E_1 + E_2\right) r^{m_1 - 1} + D_2\left(m_2 E_1 + E_2\right) r^{m_2 - 1} + \left(E_2 B_8 + E_4\right)\frac{\dot{A}_1}{r} \\ &+ \left(E_2 B_7 + E_3\right)\frac{\dot{A}_2}{r} + E_1\left(\frac{\partial G_{11}}{\partial r} r^{m_1} + G_{11} m_1 r^{m_1 - 1} + \frac{\partial G_{21}}{\partial r} r^{m_2} + G_{21} m_2 r^{m_2 - 1}\right) \\ &+ E_2\left(G_{11} r^{m_1 - 1} + G_{21} r^{m_2 - 1}\right) + \left(E_1 - E_2\right)\frac{\sqrt{3}}{2} b_0 r^{b_1} \sigma_e^{n_0} \end{aligned} \tag{32.b}$$

$$\begin{aligned} \dot{\phi} =& D_1 r^{m_1}\left(L_1 + \frac{L_2}{m_1}\right) + D_2 r^{m_2}\left(L_1 + \frac{L_2}{m_2}\right) - \left(B_8 L_2 - L_5\right)\ln(r)\dot{A}_1 - \left(B_7 L_2 + L_3\right)\ln(r)\dot{A}_2 \\ &+ \int\left(L_1\left(\frac{\partial G_{11}}{\partial r} r^{m_1} + G_{11} m_1 r^{m_1 - 1} + \frac{\partial G_{21}}{\partial r} r^{m_2} + G_{21} m_2 r^{m_2 - 1}\right)\right. \\ &\left. + L_2\left(+G_{11} r^{m_1 - 1} + G_{21} r^{m_2 - 1}\right) + \left(L_1 - L_2\right)\frac{\sqrt{3}}{2} b_0 r^{b_1} \sigma_e^{n_0}\right) dr + J_1 \end{aligned} \tag{32.c}$$

$$\begin{aligned} \dot{\psi} =& D_1 r^{m_1}\left(P_1 + \frac{P_2}{m_1}\right) + D_2 r^{m_2}\left(P_1 + \frac{P_2}{m_2}\right) - \left(B_8 P_2 + P_3\right)\ln(r)\dot{A}_1 - \left(B_7 P_2 - P_5\right)\ln(r)\dot{A}_2 \\ &+ \int\left(P_1\left(\frac{\partial G_{11}}{\partial r} r^{m_1} + G_{11} m_1 r^{m_1 - 1} + \frac{\partial G_{21}}{\partial r} r^{m_2} + G_{21} m_2 r^{m_2 - 1}\right)\right. \\ &\left. + P_2\left(+G_{11} r^{m_1 - 1} + G_{21} r^{m_2 - 1}\right) + \left(P_1 - P_2\right)\frac{\sqrt{3}}{2} b_0 r^{b_1} \sigma_e^{n_0}\right) dr + J_2 \end{aligned} \tag{32.d}$$

Using the boundary conditions, the unknown constants can be determined. The pressure, electric and magnetic potential of internal and external surface of the piezomagnetic thick-walled cylinder does not vary with the time, so we have:

$$\begin{aligned} &\dot{\sigma}_r\big|_{r=a}=0, \quad \dot{\sigma}_r\big|_{r=b}=0,\\ &\dot{\phi}\big|_{r=a}=0, \quad \dot{\phi}\big|_{r=b}=0,\\ &\dot{\psi}\big|_{r=a}=0, \quad \dot{\psi}\big|_{r=b}=0. \end{aligned} \tag{33}$$

The resultant system of linear equations can be solved like in the previous section. To achieve history of stresses, electric and magnetic potential during creep progress, the rates of stresses, electric potential and magnetic potential are needed. First of all, a suitable time increment needs to be taken for timing steps ($dt^{(i)}$). As the creep evolutions during the time, the sum of time steps is the total time. The total time after the i_{th} timing step can be presented as:

$$t_i=\sum_{k=0}^{i} dt^{(\text{k})} \tag{34}$$

In the following time increments, the distributions of the radial and hoop stress for former step are available, and then, the radial and hoop stress rates are acquired from Eqs (33.a) and (33.b). Lastly, using an iterative method, the creep stress distribution can be achieved as:

$$\begin{aligned} \sigma_r^{(\text{i})}(\text{r},\text{t}_i)=\sigma_r^{(\text{i}-1)}(\text{r},\text{t}_{i-1})+\dot{\sigma}_r^{(\text{i}-1)}(\text{r},\text{t}_{i-1})\,\text{dt}^{(\text{i})}\\ \sigma_\theta^{(\text{i})}(\text{r},\text{t}_i)=\sigma_\theta^{(\text{i}-1)}(\text{r},\text{t}_{i-1})+\dot{\sigma}_\theta^{(\text{i}-1)}(\text{r},\text{t}_{i-1})\,\text{dt}^{(\text{i})} \end{aligned} \tag{35}$$

4. Numerical Results and Discussions

To explore the effect of parameters on the response of piezomagnetic cylinder, some numerical examples are presented here. Material properties for the piezomagnetic are presented in Table 1 [4, 34]. The interior and exterior radius of the hollow cylinder is considered as a=0.1m and b=0.4m, respectively. The following non-dimensional quantities are used for the numerical results:

$$R=\frac{r-a}{b-a}, \quad u^*=\frac{u(r)}{a}, \quad \sigma_i^*=\frac{\sigma_i}{P_a}, (i=r,\theta), \quad \phi^*=\sqrt{\frac{\beta_{11}}{c_{11}}}\frac{\phi(r)}{b}, \quad \psi^*=\sqrt{\frac{d_{11}}{c_{11}}}\frac{\psi(r)}{b}. \tag{36}$$

Firstly, the creep evolution during the time is investigated. The multiphysical boundary conditions are considered as:

$$P_a=10\,MPa, \quad \phi_a=0, \quad \phi_b=3000, \quad \psi_a=0, \quad \psi_b=0, \quad T_a=30, \quad T_b=0, \quad M_a=0.5, \quad M_b=0 \tag{37}$$

Table 1. Material constants.

$c_{11}\,(GPa)$	$c_{12}\,(GPa)$	$c_{23}\,(GPa)$	$c_{22}\,(GPa)$	$e_{11}\,(C/m^2)$
215	120	120	218	7.5
$e_{12}\,(C/m^2)$	$\alpha_r(1/K)$	$\alpha_\theta(1/K)$	$q_{11}\,(N/Am)$	$q_{12}\,(N/Am)$
-2.5	6×10^{-6}	15×10^{-6}	345	265
$\beta_{11}(C^2/Nm^2)$	$d_{11}(Ns^2/C^2)$	$\varepsilon_{11}(Ns/VC)$	$\beta_r(m^3/kg)$	$\beta_\theta(m^3/kg)$
5.8×10^{-9}	95×10^{-6}	2.82×10^{-9}	0.8×10^{-4}	1.2×10^{-4}
$m_1(N/AmK)$	$\chi_1(Cm/kg)$	$P_1(C^2/m^2k)$	$\gamma_1(Nm^2/Akg)$	n_0
2.5×10^{-5}	0	-2.5×10^{-5}	0	3
b_1	b_0			
-5	0.11×10^{-36}			

Figure 2 shows the creep evolution of hollow piezomagnetic cylinder. In this research, the time increment $dt=5\times10^4$s is used. As observed, the radial stress, electric potential and magnetic potential do not change with time at the inside and outside surface of the cylinder which satisfies the constant electro-magneto-mechanical boundary conditions. Figure 2(a) shows the radial stress, in the most part of thickness, rises with the time. Figure 2(b) depicts that the positive hoop stress rises with time in the most part of the thickness, while the negative hoop decreases at the interior surface. Since the hoop stress becomes maximum at the outside surface, the increase in tensile hoop stress at the outside surface must be considered in design progress because the huge tensile hoop stress results in cracking [30]. According to Fig. 2(c), the equivalent stress increases with time. However, the enhancement is smaller at the internal radius rather than other parts of the thickness. Figure 2(d) reveals that outward radial displacement rises with time. However, the increase is more significant near the inner radius. Figure 2(e) illustrates that the maximum electric potential decreases with time initially. After that, the direction of the curvature of the graph is reversed and so the maximum electric potential increases with time in the opposite direction. Concerning to Fig. 2(f), the positive part of magnetic potential decreases with time; conversely, the negative part increases.

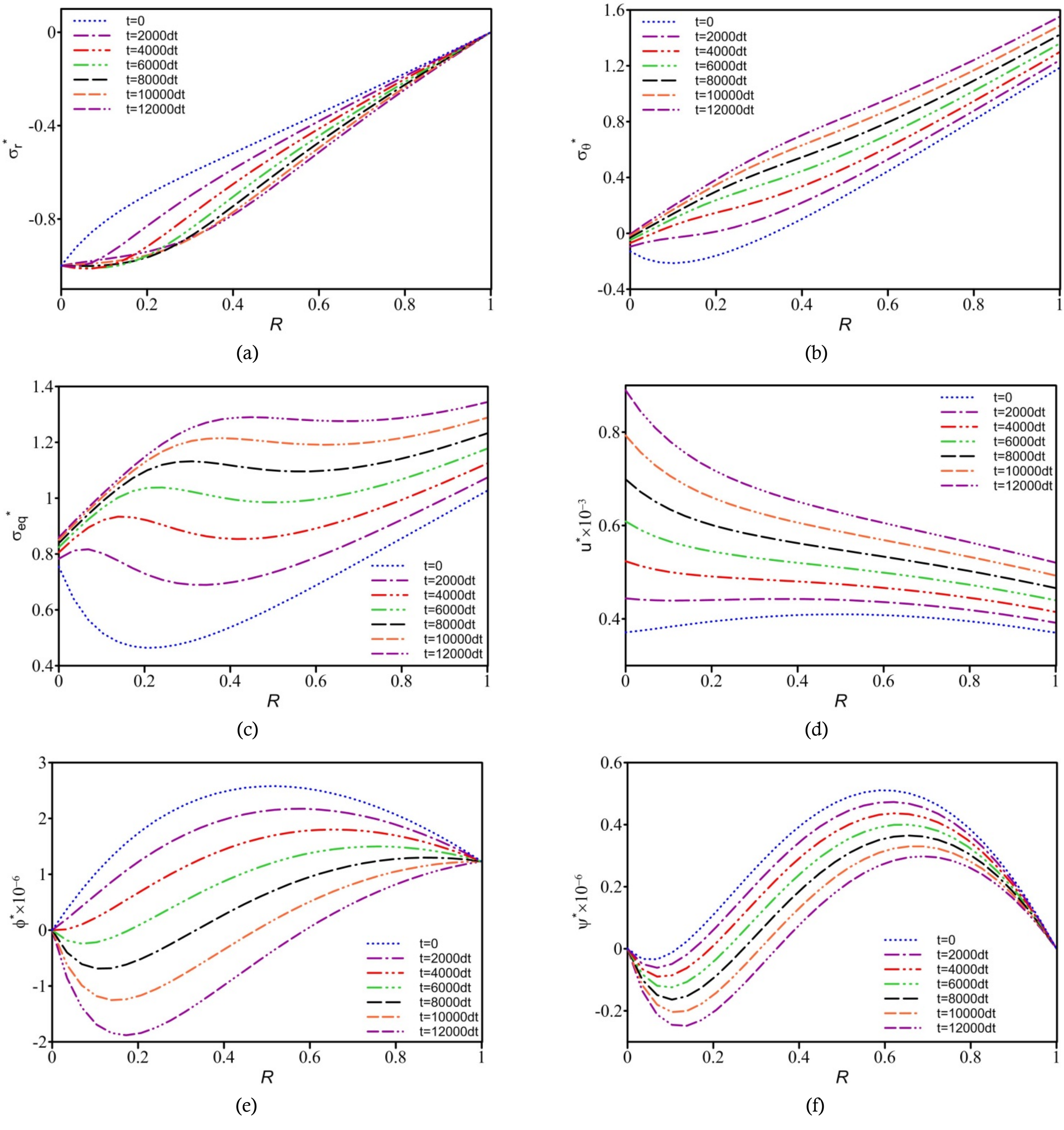

Fig. 2. (a) Radial, (b) hoop and (c) equivalent creep stresses, (d) radial displacement (e) electric and (f) magnetic potentials redistribution during creep progress

The effect of temperature and humidity on the primitive and creep behavior of the piezomagnetic cylinder is shown in Fig. 3. The temperature and moisture concentrations at the outer radius are kept at zero. However, the temperature and moisture concentration increase at the inner radius. Other boundary conditions are similar to the previous case. According to Fig. 3(a), rising in hygrothermal loading rises the initial compressive radial stress. Moreover, the tensile creep radial stress is changed to compressive by rising in hygrothermal loading. Figure 3(b) depicts that, for primitive case, there is a fixed point near the middle of the thickness in which the hoop stress has no change with changes in hygrothermal loading. Before this point, rising in hygrothermal loading reduces the circumferential stress. Conversely, after this point, it increases the circumferential stress. The primitive equivalent stress also shows a similar behavior as can be seen in Fig. 3(c). Besides, by rising in hygrothermal loading, the location of maximum initial hoop stress is changed from inner radius to outer radius. For the creep case, increasing in hygrothermal loading decreases the hoop stress at most part of the thickness. The changes are more significant at the outer radius. Furthermore, the similar behavior for the creep equivalent stress can be seen.

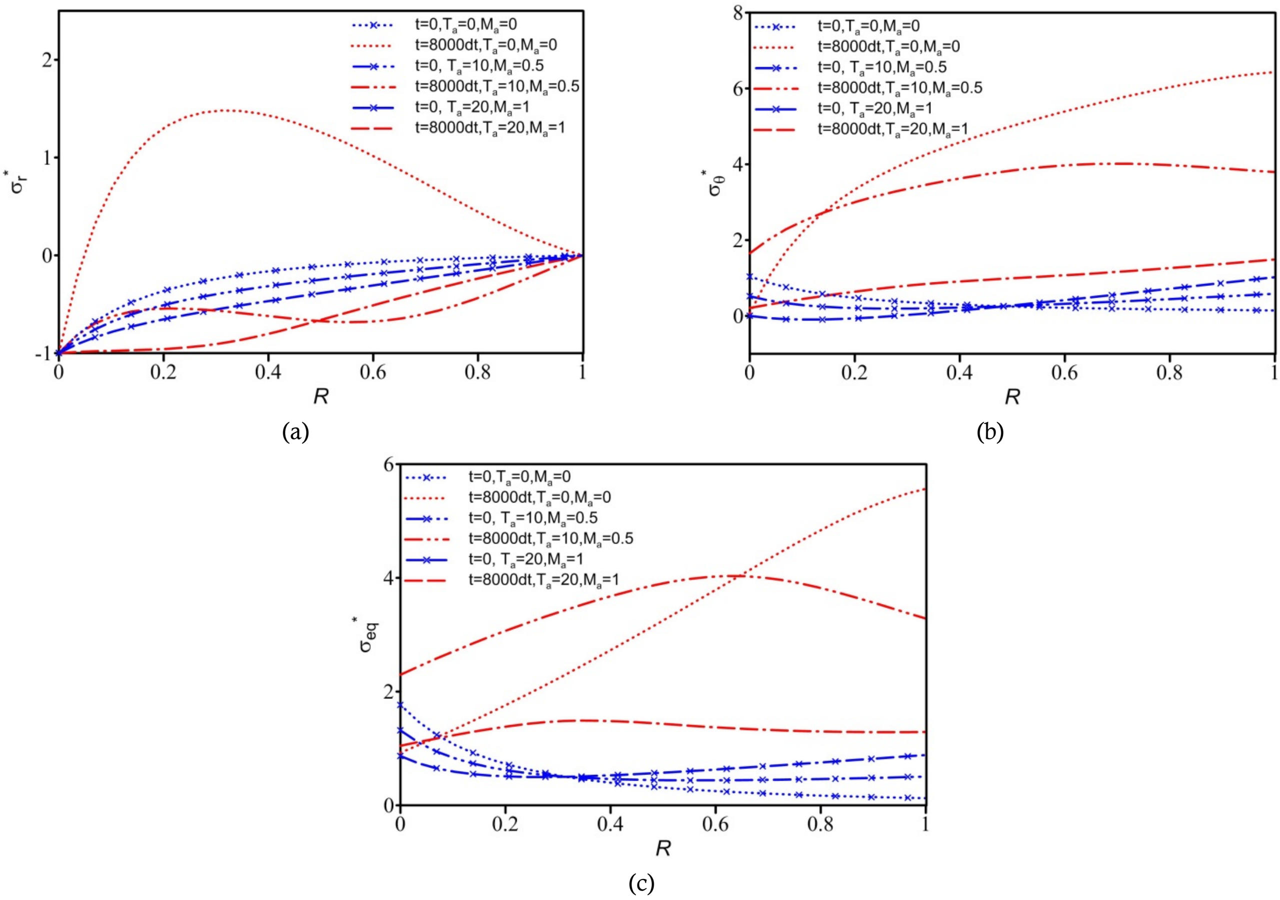

Fig. 3. Effect of hygrothermal loading on the primitive and creep (a) Radial, (b) hoop and (c) equivalent creep stresses redistributions

To reveal the effect of dependency of the elastic coefficients to temperature and moisture on the behavior of piezomagnetic cylinder, the elastic coefficients can be assumed in the form as [14]:

$$C_{ij} = C_{ij0}(1+\alpha^{*}\,\mathrm{T}+\beta^{*}\,\mathrm{M}) \tag{38}$$

To avoid having non-linear equations, temperature and moisture concentration are assumed to increase just uniformly. Therefore, the temperature and moisture concentration rises uniformly as: T=30, M=0.5. Other boundary conditions are kept unchanged. Owing to similarity of the effect of the temperature and moisture concentration, the similar magnitudes are used for the empirical constants of temperature and moisture dependence. It should be noted that $\alpha^*=\beta^*=0$ indicates the material properties that are independent of temperature and moisture. Figure 4(a) depicts the initial radial stress increases by using a positive magnitude of the empirical constant and conversely decreases by using a minus value. While, after creep evolution, the radial stress shows an opposite behavior. According to Fig. 4(b), there is a fixed point that the primitive circumferential stress is not dependent to the value of empirical constant. Before this point, minus value of empirical constant results in an increase in hoop stress. While, after the point, it results in a reduction. The effect of positive value of empirical constant is vice versa. Also, the creep hoop stress rises using negative empirical constant. Whereas, it decreases using positive value of empirical constant. The same behavior as the hoop stress can be seen in the equivalent stress according to Fig. 4(c). Figure 4(d) shows the minus value of empirical constants results in a rising in radial displacement of each point. While the positive value has a reverse effect. Figure 4(d), (e) and (f) show that the effect of the value of empirical constant on the radial displacement, electric potential and magnetic potential of the piezomagnetic cylinder is more significant after the creep progress rather than the initial one. Figure 4 implies the creep analysis is vital for the materials that their properties are dependent on temperature and moisture.

Angular velocity is the next effective parameter is considered in this paper. In this case, T_a=30, M_a=0.5 and other parameters are as before. The results are demonstrated in Fig. 5. Figure 5(a) shows that increasing in angular velocity leads to reduction in initial radial stress. The decline increases by increasing in angular velocity. Besides, increasing in angular velocity results in increase in creep radial stress in most part of the thickness. Figure 5(b) depicts that both initial and creep hoop stresses increase at an increasing rate by increasing in angular velocity. The change in creep case is more significant comparison with the initial case. The general behavior of the equivalent stress is same as the hoop stress as observed in Fig. (c). Concerning Fig. 5(d), rising in angular velocity results in an increase in the both initial and creep radial displacement. However, the enhancement is more extensive for the creep case. According to Fig. 5 (e) and (f), as the angular velocity rises, the electric potential and magnetic potential increase in creep case. While, the effect of angular velocity on the electric potential and magnetic potential in initial case is insignificant.

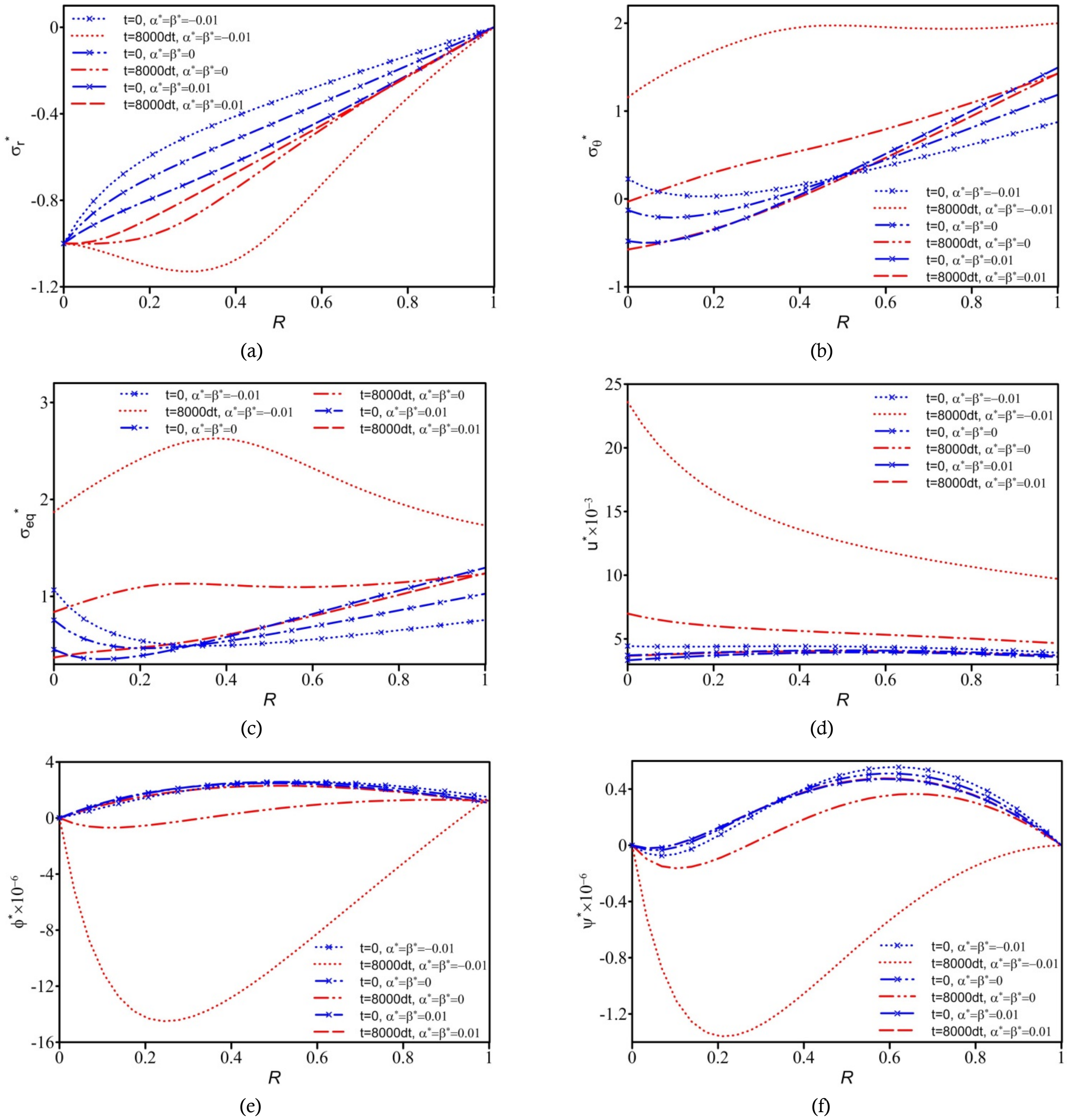

Fig. 4. Effect of temperature and moisture dependency on the primitive and creep (a) Radial, (b) hoop and (c) equivalent creep stresses, (d) radial displacement (e) electric and (f) magnetic potentials redistributions

The distribution of stresses and radial displacement of piezomagnetic cylinder subjected to different loading types are shown in Fig. 6. In this case ω=20π and other conditions are similar to the before case. According to Fig. 6(a), the radial stresses caused by the rotation and magnetic potential are tensile. While, the radial stresses caused by the internal pressure, moisture concentration and thermal loading are compressive. However the effect of electric potential is not considerable. Figure 6(b) shows that at the external surface in which the hoop stress is maximum, the thermal loading is the most effective loading. While, at the internal surface, thermal loading and internal pressure are the most effective loadings. At the external loading only the hoop stress caused by magnetic potential is negative. Figure 6(c) depicts that the radial displacement caused by magnetic potential is inward. While, the radial displacement caused by electric potential is negligible and the radial displacement caused by other loading types are outward. The most effective loadings on the radial displacement are the thermal and internal pressure loadings.

To the best of author's knowledge, there is no reported research in the literature for time-dependent creep analysis of MEE cylinders. However, static analysis of rotating MEE hollow cylinder has been carried out by Ref. [12]. So, to validate the results, the radial stress distribution for different angular velocity is shown in the Fig. 7. The details of non-dimensional parameters and material constants can be found in Ref. [12]. As observed, good agreement can be found between the results.

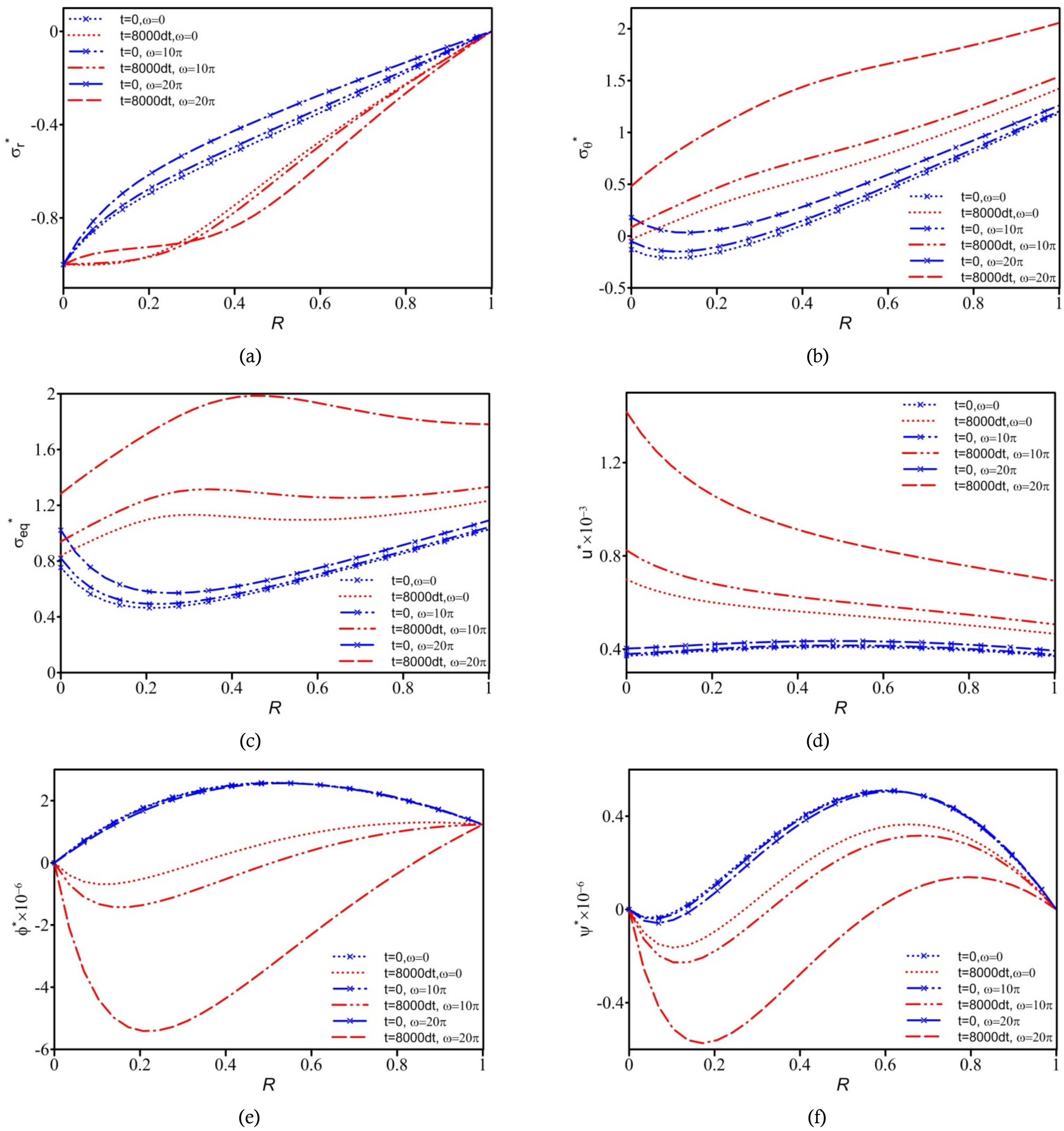

Fig. 5. Effect of speed of rotation on the (a) Radial, (b) circumferential and (c) equivalent creep stresses, (d) radial displacement (e) electric and (f) magnetic potentials redistribution during creep progress

5. Conclusion

An analytical solution for the time-dependent creep problem of a piezomagnetic hollow cylinder subjected to an axisymmetric multiphysical loading is presented. The Prandtl-Reuss equations and Norton's law are used in this analysis. The following conclusions are found in this research:

- The radial and hoop stresses, in the most part of thickness, as well as the equivalent stress and outward radial displacement rise with time during the creep evolution.
- Since the maximum positive hoop stress rises at the outside surface during the creep progress, this increase must be considered in design progress because the huge tensile hoop stress results in cracking.
- The results imply the creep analysis is vital for the materials that their properties are dependent on temperature and moisture because the effect of temperature- and moisture-dependency is more significant after creep progress rather than the initial case.
- As the angular velocity increases, the hoop stress, equivalent stress, radial displacement, electric potential and

magnetic potential increase after creep evolution. The changes after creep evolution are more extensive rather than the primitive state.

- The results imply that the effect of internal hygrothermal loading is more extensive after creep evolution comparison with the initial state.

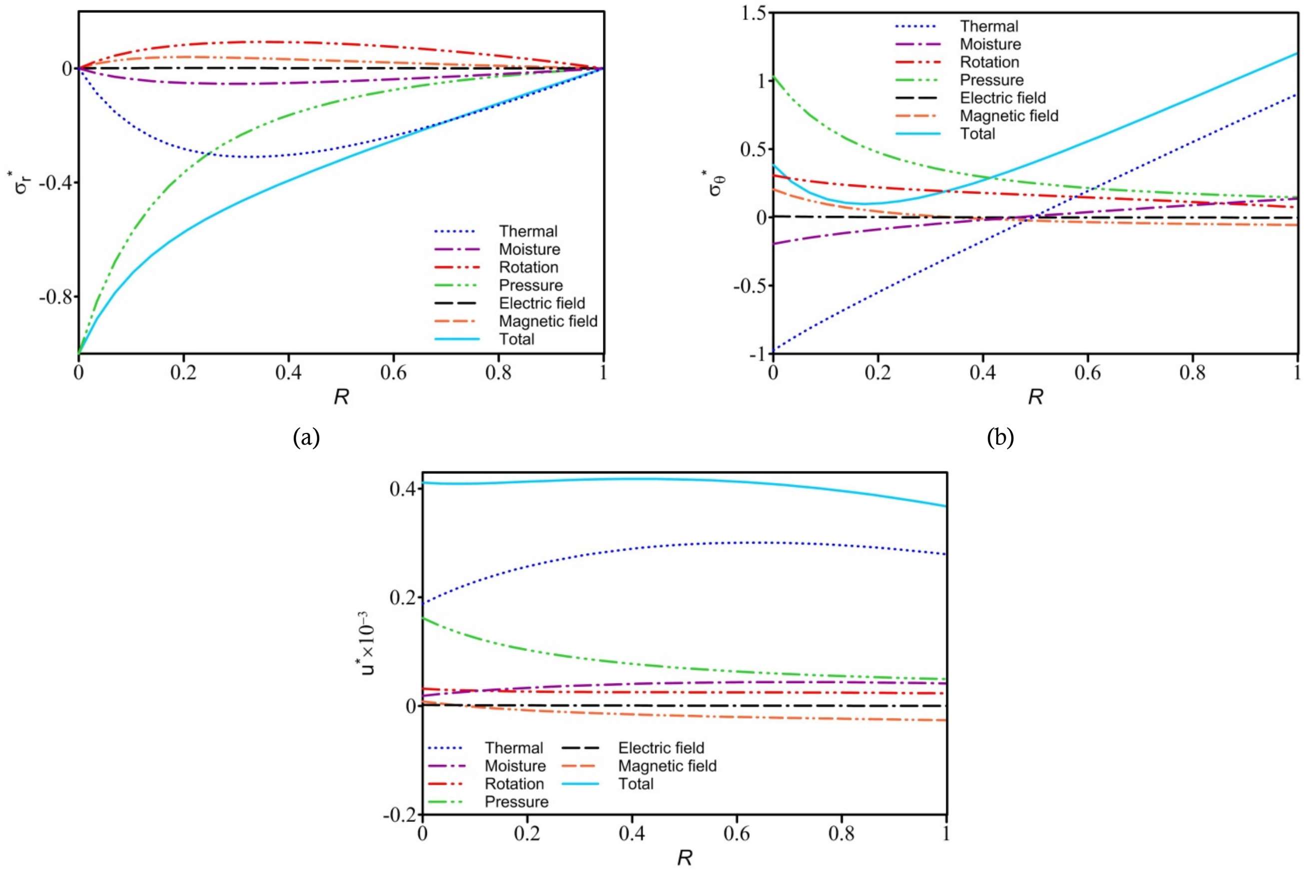

(a) (b) (c)

Fig. 6. The initial (a) Radial, (b) hoop and (c) radial displacement distributions

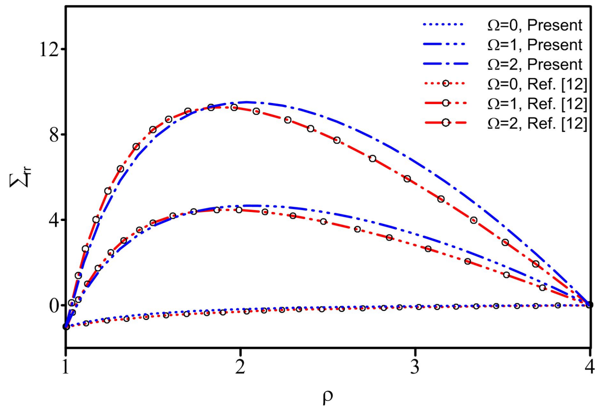

Fig. 7. Radial stress

Conflict of Interest

The author declared no potential conflicts of interest with respect to the research, authorship and publication of this article.

Funding

The author received no financial support for the research, authorship and publication of this article.

Nomenclature

B_r	Magnetic induction	β_i	Moisture expansion coefficients
C_{ij0}	Temperature and moisture independent elastic coefficient	β^*	Empirical material coefficient for moisture dependence
c_{ij}	Elastic coefficients	γ_1	Hygromagnetic coefficient
D_r	Electric displacement	ε_{11}	Electromagnetic coefficient
d_{11}	Magnetic coefficient	$\dot{\varepsilon}_i^c$	Creep strain rate
e_{1j}	Piezoelectric coefficient	$\dot{\varepsilon}_e^c$	Effective creep strain rate
k^C	Moisture diffusivity coefficient	ς_i	Hygroscopic stress coefficients
k^T	Thermal conductivity coefficient	ρ	Density
m_1	Pyromagnetic coefficient	σ_e	Effective stress
p_1	Pyroelectric coefficient	σ_i	Stresses
q_{1j}	Piezomagnetic coefficient	ϕ	Electric potential
α_i	Thermal modulus coefficients	χ_1	Hygroelectric coefficient
α^*	Empirical material coefficient for temperature dependence	ψ	Magnetic potential
β_{11}	Dielectric coefficient		

References

[1] Smittakorn, W., Heyliger, P.R., A discrete-layer model of laminated hygrothermopiezoelectric plates, *Mechanics of Composite Materials and Structures,* 7, 2000, 79-104.

[2] Raja, S., Sinha, P.K., Prathap, G., Dwarakanthan, D., Thermally induced vibration control of composite plates and shells with piezoelectric active damping, *Smart Materials and Structures,*13, 2004, 939-950.

[3] Allam, M.N.M., Zenkour, A.M., Tantawy, R., Analysis of Functionally Graded Piezoelectric Cylinders in a Hygrothermal Environment, *Advances in Applied Mathematics and Mechanics,* 6, 2014, 233-246.

[4] Saadatfar, M., Aghaie-Khafri, M., Hygrothermomagnetoelectroelastic analysis of a functionally graded magneto-electro-elastic hollow sphere resting on an elastic foundation, *Smart Materials and Structures,* 23, 2014, 1-13.

[5] Saadatfar, M., Aghaie-Khafri, M., Hygrothermal analysis of a rotating smart exponentially graded cylindrical shell with imperfect bonding supported by an elastic foundation, *Aerospace Science and Technology,* 43, 2015, 37-50.

[6] Saadatfar, M., Aghaie-Khafri, M., On the behavior of a rotating functionally graded hybrid cylindrical shell with imperfect bonding subjected to hygrothermal condition, *Journal of Thermal Stresses,* 38, 2015, 854-881.

[7] Saadatfar, M., Effect of multiphysics conditions on the behavior of an exponentially graded smart cylindrical shell with imperfect bonding, *Meccanica,* 50, 2015, 2135–2152.

[8] Zenkour, A.M., Bending analysis of piezoelectric exponentially graded fiber-reinforced composite cylinders in hygrothermal environments, *International Journal of Mechanics and Materials in Design,* 13, 2017, 515-529.

[9] Vinyas, M., Kattimani, S., Hygrothermal Analysis of Magneto-Electro-Elastic Plate using 3D Finite Element Analysis, *Composite Structures,* 180, 2017, 617-637.

[10] Hou, P.F., Leung, A.W.T., The transient responses of magneto-electro-elastic hollow cylinders. *Smart Materials and Structures,* 13, 2004, 762.

[11] Wang, H.M., Ding, H.J., Transient responses of a special non-homogeneous magneto-electro-elastic hollow cylinder for a fully coupled axisymmetric plane strain problem, *Acta Mechanica,* 184, 2006, 137–157.

[12] Babaei, M.H., Chen, Z.T., Exact solutions for radially polarized and magnetized magneto electro elastic rotating cylinders, *Smart Materials and Structures,* 17, 2008, 025035.

[13] Ootao, Y., Ishihara, M., Exact Solution of Transient Thermal Stress Problem of a Multilayered Magneto-Electro-Thermoelastic Hollow Cylinder, *Applied Mathematical Modelling,* 5, 2011, 90-103.

[14] Akbarzadeh, A.H., Chen, Z.T., Magnetoelectroelastic behavior of rotating cylinders resting on an elastic foundation under hygrothermal loading, *Smart Materials and Structures,* 21, 2012, 125013.

[15] Loghman, A., Ghorbanpour Arani, A., Amir, A.S., Vajedi, A., Magnetothermoelastic creep analysis of functionally graded cylinders, *International Journal of Pressure Vessels and Piping*, 87, 2011, 389-395.

[16] Singh, T., Gupta, V.K., Effect of anisotropy on steady state creep in functionally graded cylinder, *Composite Structures*, 93, 2011, 747-758.

[17] Sharma, S., Sahay, I., Kumar, R., Creep transition in non homogeneous thick-walled circular cylinder under internal and external pressure, *Applied Mathematical Sciences*, 122, 2012, 6075-6080.

[18] Loghman, A., Atabakhshian, V., Semi-analytical solution for time-dependent creep analysis of rotating cylinders made of anisotropic exponentially graded material (EGM), *Journal of Solid Mechanics*, 4, 2012, 313-326.

[19] Jamian, S., Sato, H., Tsukamoto, H., Watanabe, Y., Creep analysis of functionally graded material thick-walled cylinder, *Applied Mechanics and Materials*, 315, 2013, 867-871.

[20] Nejad, M.Z., Kashkoli, M.D., Time-dependent thermo-creep analysis of rotating FGM thick-walled cylindrical pressure vessels under heat flux, *International Journal of Engineering Science,* 82, 2014, 222–237.

[21] Singh, T., Gupta, V.K., Analysis of steady state creep in whisker reinforced functionally graded thick cylinder

subjected to internal pressure by considering residual stress, *Mechanics of Advanced Materials and Structures*, 21, 2014, 384-392.
[22] Nejad, M.Z., Hoseini, Z., Niknejad, A., Ghannad, M., Steady-state creep deformations and stresses in FGM rotating thick cylindrical pressure vessels, *Journal of Mechanics*, 31, 2015, 1-6.
[23] Kashkoli, M.D., Tahan, K.N., Nejad, M.Z., Time-dependent thermomechanical creep behavior of FGM thick hollow cylindrical shells under non-uniform internal pressure, *International Journal of Applied Mechanics*, 9, 2017, 750086.
[24] Kashkoli, M.D., Tahan, K.N., Nejad, M.Z., Time-dependent creep analysis for life assessment of cylindrical vessels using first order shear deformation theory, *Journal of Mechanics*, 33, 2017, 461-474.
[25] Sharma, S., Yadav, S., Sharma, R., Thermal creep analysis of functionally graded thick-walled cylinder subjected to torsion and internal and external pressure, *Journal of Solid Mechanics*, 9, 2017, 302-318.
[26] Bakhshizadeh, A., Nejad, M.Z., Kashkoli, M.D., Time-Dependent Hygro-Thermal Creep Analysis of Pressurized FGM Rotating Thick Cylindrical Shells Subjected to Uniform Magnetic Field, *Journal of Solid Mechanics,* 9, 2017, 663-679.
[27] Ghorbanpour Arani, A., Kolahchi, R., Mosallaie Barzoki, A.A., Loghman, A., Time-Dependent Thermo-Electro-Mechanical Creep Behavior of Radially Polarized FGPM Rotating Cylinder, *Journal of Solid Mechanics,* 3, 2011, 142-157.
[28] Ghorbanpour Arani, A., Mosallaie Barzoki, A.A., Kolahchi, R., Mozdianfard, M.R., Loghman, A., Semi-analytical solution of time-dependent electro-thermo-mechanical creep for radially polarized piezoelectric cylinder, *Computers and Structures,* 89, 2011, 1494–1502.
[29] Saadatfar, M., Aghaie-Khafri, M., On the magneto-thermo-elastic behavior of a FGM cylindrical shell with pyroelectric layers featuring interlaminar bonding imperfections rested in an elastic foundation, *Journal of Solid Mechanics,* 7, 2015, 344-363.
[30] Saadatfar, M., Razavi, A.S., Piezoelectric hollow cylinder with thermal gradient, *Journal of Mechanical Science and Technology,* 23, 2009, 45-53.
[31] Chang, W.J., Transient hygrothermal responses in a solid cylinder by linear theory of coupled heat and moisture, *Applied Mathematical Modelling,* 18, 1994, 467-473.
[32] Saadatfar, M., Aghaie-Khafri, M., Thermoelastic analysis of a rotating functionally graded cylindrical shell with functionally graded sensor and actuator layers on an elastic foundation placed in a constant magnetic field, *Journal of Intelligent Materials Systems and Structures,* 27, 2015, 512-527.
[33] Saadatfar, M., Effect of Interlaminar Weak Bonding and Constant Mag-netic Field on the Hygrothermal Stresses of a FG Hybrid Cylindrical Shell Using DQM, *Journal of Stress Analysis*, 3, 2018, 93-110.
[34] Dai, H.L., Jiang, H.J., Yang, L., Time-dependent behaviors of a FGPM hollow sphere under the coupling of multi-fields Solid State Sciences, *Solid State Sciences,* 14, 20112, 587-597.
[35] Loghman, A., Abdollahian, M., Jafarzadeh Jazi, A., Ghorbanpour Arani, A., Semi-analytical solution for electromagnetothermoelastic creep response of functionally graded piezoelectric rotating disk, *International Journal of Thermal Sciences,* 65, 2013, 254-266.